

# On the accreting tori sequences in Ringed Accretion Disks models. Polytropic equations of state and toroidal magnetic fields

Daniela Pugliese<sup>1,a</sup> and Zdeněk Stuchlík<sup>1,b</sup>

<sup>1</sup>Institute of Physics and Research Centre of Theoretical Physics and Astrophysics,  
 Faculty of Philosophy & Science, Silesian University in Opava,  
 Bezručovo náměstí 13, CZ-74601 Opava, Czech Republic

<sup>a</sup>d.pugliese.physics@gmail.com

<sup>b</sup>zdenek.stuchlik@physics.cz

## ABSTRACT

We consider ringed accretion disks (**RADs**), representing models of aggregates of corotating and counterrotating toroids orbiting a central Kerr super-massive black hole (**SMBH**). We comment on system of two-tori governed by the polytropic equation of state and including a toroidal magnetic field. We found the **RADs** leading function describing the **RAD** inner structure and governing the distribution of orbiting toroidal structures and the emergence of the (hydro-mechanical) instabilities in the disk. We perform this analysis first in pure hydrodynamical models by considering one-specie perfect fluid toroids and then by considering the contribution of toroidal magnetic field.

**Keywords:** Accretion; Accretion disks; Black holes; Active Galactic Nuclei (AGN)

## 1 INTRODUCTION

Active Galactic Nuclei (**AGNs**) provide a rich scenario to observe **SMBHs** interacting with their environments. Chaotical, discontinuous accretion episodes may leave traces in the form of matter remnants orbiting the central attractor producing sequences of orbiting toroidal structures with strongly different features as different rotation orientations with respect to the Kerr **BH** where corotating and counterrotating accretion stages can be mixed.

Motivated by these facts, ringed accretion disks (**RADs**) model structured toroidal disks which may be formed during several accretion regimes occurred in the lifetime of non-isolated Kerr **BHs**. **RAD** features a system made up by several axi-symmetric matter configurations orbiting in the equatorial plane of a single central Kerr **SMBH**. Both corotating and counterrotating tori are possible constituents of the **RADs**. This model was first introduced in Pugliese and Montani (2015) and then detailed in Pugliese and Stuchlík (2015,

2016, 2017); Pugliese and Stuchlík (2018c,b,a); Pugliese and Stuchlík (2019); Pugliese and Montani (2018).

The model strongly binds the fluid and **BH** characteristics providing indications on the situations where to search for **RADs** observational evidences. The number of the instability points is generally limited to  $n=2$  and depends on the dimensionless spin of the rotating central attractor. The phenomenology associated with these toroidal complex structures may be indeed very wide, providing a different interpretative framework. Obscuring and screening tori, possibly evident as traces (screening) in x-ray spectrum emission, are also strongly constrained. More generally, observational evidence is expected by the spectral features of **AGNs** X-ray emission shape, due to X-ray obscuration and absorption by one of the tori, providing a **RAD** fingerprint as a radially stratified emission profile.

In Sec. (2) we introduce the model and the main definitions used throughout this article. In Sec. (2.1) we focus on **RAD** with polytropic tori. In Sec. (3) we analyze the effects of a toroidal magnetic field in the formation of several magnetized accretion tori. Concluding remarks are in Sec. (4). Appendix (A) summarizes main constraints on the **RAD** structure.

## 2 RINGED ACCRETION DISKS

Ringed accretion disk (**RAD**) is a fully general relativistic model of axially symmetric but "knobby" accretion disk orbiting on the equatorial plane of a Kerr **SMBH**. It is constituted by an aggregate of corotating and counter-rotating perfect fluid, one particle species, tori orbiting on the equatorial plane on one central **BH** attractor. Because of the symmetries of the system (stationarity and axial-symmetry) the system is regulated by the Euler equation only with a barotropic equation of state (**EoS**)  $p = p(\varrho)$ :

$$T_{\mu\nu} = (p + \varrho)U_\mu U_\nu - pg_{\mu\nu}, \quad \frac{\nabla_\mu p}{p + \varrho} = -\nabla_\mu \ln(U_t) + \frac{\Omega \nabla_\mu \ell}{1 - \Omega \ell} \quad (1)$$

$$\Omega = \frac{U^\phi}{U^t} = -\frac{g_{t\phi}}{g_{\phi\phi}}\ell_0 = \frac{f(r)}{r^2 \sin^2 \theta}\ell_0, \quad \ell = -\frac{U_\phi}{U_t}. \quad V_{eff}(\ell) \equiv u_t \quad W \equiv \ln V_{eff}(\ell),$$

(( $t, r, \phi, \theta$ ) are Boyer-Lindquist coordinates), where  $V_{eff}(\ell)$  is the torus effective potential,  $\Omega$  is the fluid relativistic angular frequency,  $\ell$  specific angular momenta, assumed constant and conserved for each **RAD** component but variable in the **RAD** distribution,  $U^a$  is the fluid four velocity,  $T_{\mu\nu}$  is the fluid energy momentum tensor.

We introduce the following definitions: we use the notation () to indicate a configuration which can be closed, C, or open O. Specifically, toroidal surfaces correspond to the equipotential surfaces, critical points of  $V_{eff}(\ell)$  as function of  $r$ , thus solutions of  $W : \ln(V_{eff}) = c = \text{constant}$  or  $V_{eff} = K = \text{constant}$  where **C**—cross sections of the closed surfaces (equilibrium quiescent torus); **C<sub>×</sub>**—cross sections of the closed cusped surfaces (accreting torus); **O<sub>×</sub>**—cross sections of the open cusped surfaces, generally associated to proto-jet configurations Pugliese and Stuchlík (2018a); Pugliese and Stuchlík (2016). Sign  $Q_\pm$  for a general quantity  $Q$  refers to counterrotating and corotating tori respectively. We introduce the concept of  $\ell$ corotating disks, defined by the condition  $\ell_{(i)}\ell_{(o)} > 0$ , and  $\ell$ counterrotating disks defined by the relations  $\ell_{(i)}\ell_{(o)} < 0$ . The two  $\ell$ corotating tori can be

both corotating,  $\ell a > 0$ , or counterrotating,  $\ell a < 0$ , with respect to the central attractor spin  $a > 0$ . We use short notation  $O_i < O_o$  and  $O_o > O_i$  for the inner and outer configurations of a **RAD** couple.

An essential part of the **RAD** analysis is the characterization of the boundary conditions on each torus in the agglomerate and of the **RAD** disk inner structure. The model is constructed investigating the function representing the angular momentum distribution inside the disk (which is not constant), which sets the toroids location (and equilibrium) in the agglomerate and it coincides, in the hydrodynamical **RAD** model of perfect fluids, with the distribution of specific angular momentum of the fluid in each agglomerate toroid. This function can be written as

$$\text{Leading (HD) RAD function} \quad \pm \ell^\mp = \pm \frac{a^3 + ar(3r - 4M) \mp \sqrt{r^3 \Delta^2}}{a^2 - (r - 2M)^2 r} \Big|_{r^*}, \quad (2)$$

$$\Delta \equiv r^2 - 2Mr + a^2,$$

( $M$  is the central **BH** mass). Each point  $r > r_{mso}$  (marginally stable orbit) on curve  $\ell^\mp$  fixes the center (points of maximum density inside the torus) of the toroidal **RAD** component,  $r < r_{mso}$  sets possible instabilities points of the toroids, more details can be found in Pugliese and Stuchlik (2015, 2017). Because of the importance of this function in defining the inner structure of the **RAD** this is called Leading **RAD** function. We shall see in Sec. (3) that, by changing the energy momentum tensor including for example a toroidal magnetic field, it will be convenient to change the leading function  $\ell^\pm$  adopted in the Hydrodynamical (HD) case to a different function, obtained through the study of the magnetic field in the **RAD** and able to represent and regulate the tori distribution. In Sec. (A) we include a summary of the main constraints on the **RAD** inner structure—Pugliese and Stuchlik (2015, 2017)

## 2.1 Polytropic tori

We conclude this section, considering **RAD** tori with polytropic fluids:  $p = \kappa \varrho^{1+1/n}$ . We develop some general considerations on the **EoS** and the polytropic **RAD** tori governed by the **EoS**:  $p = \kappa \varrho^\gamma$ , where  $\kappa > 0$  is a constant and  $\gamma = 1 + 1/n$  is the polytropic index, in Pugliese et al. (2013). Details on this analysis can be found in Pugliese and Stuchlik (2019) we also refer to this analysis for a comment on the tori energetics of various **RAD** configurations, and significance in the case of polytropic tori. It has been shown in Pugliese et al. (2013); Pugliese and Stuchlik (2019) that for the Schwarzschild geometry ( $a = 0$ ) there is a specific classification of eligible geometric polytropics and a specific class of polytropics is characterized by a discrete range of values for the index  $\gamma$ . Therefore, we can propose a general classification for the tori ( $C, C_\times$ ), as for proto-jets  $O_\times$ , assuming a particular representation of the density function. We can write the density  $\varrho$  as function  $\gamma$ . However, we concentrate our attention on the **RAD** components  $C$  and  $C_\times$  for which

$K < 1$ , there is :

$$\begin{aligned} \varrho_\gamma &\equiv \kappa^{1/(\gamma-1)} \bar{\varrho}_\gamma \quad \text{and} \quad \bar{\varrho}_\gamma \equiv \left[ \frac{1}{\kappa} \left( V_{eff}^{-\frac{\gamma-1}{\gamma}} - 1 \right) \right]^{\frac{1}{(\gamma-1)}} \quad \text{for} \\ \gamma \neq 1 \quad \text{with} \quad \varrho_\gamma &\equiv \mathbb{C}^{1/(-1+\gamma)}, \quad \mathbb{C} \equiv (V_{eff}^{-2})^{\frac{\gamma-1}{2\gamma}} - 1. \end{aligned} \quad (3)$$

(note  $\mathbb{C}$  is actually a function of  $K \in ]K_{\min}, K_{\max}]$ , while  $K_{\max} < 1$ , regulates whether the torus is quiescent or in accretion). The pressure  $p$ , associated to the solution in Eq. (3), depends on  $\kappa^{\frac{1}{1-\gamma}}$ . It decreases with  $\kappa$  more slowly than  $\varrho$ .

We consider the case  $K < 1$  with the condition  $\varrho > 0$ , verified, according to Eq. (3), for  $\gamma > 1$ . Integration of the  $\varrho$  density function in the polytropic case where  $\gamma = 4/3$  is shown in Figs (1). The situation for different indices, and particularly  $\gamma = 5/3$ , is also shown, integration of density profiles have been specified particularly for the couple  $C_\times^- < C_\times^+$ . Note that we can then directly impose several constraints for the density function. Some simple examples, including special (composite) density profiles are, for example, the case  $\varrho_{[+]}^- = \varrho_\gamma^i - \varrho_\gamma^o = \varrho_\Phi = \text{constant}$ , where

$$K_i = \left( \left[ \varrho_\Phi - \epsilon \left( K_o^{-\frac{\gamma-1}{\gamma}} - 1 \right)^{\frac{1}{\gamma-1}} \right]^{\gamma-1} + 1 \right)^{-\frac{\gamma}{\gamma-1}}.$$

In Figs (1) we show also the profiles  $\varrho_\Phi$  for  $\epsilon = -1$ . Importantly, we note that these relations should be generally seen as constraints on *independent* solutions for each **RAD** components. Toroidal configurations emerging from these constraints ( $\varrho_{[+]}^-$ ) as in Fig (1) are by no means directly matched with solutions for two different **RAD** components coupled only through the background. The **RADs** effective potential (a potential describing the entire macrostructure as introduced in Pugliese and Stuchlík (2015)) may be derived from composite energy-momentum tensors made by collections of the fluid tensors decomposed in each fluid adapted frame. This holds for not colliding tori. They will be naturally coupled through the unique background metric tensor  $g_{\mu\nu}$  and proper boundary conditions imposed on the fluid density and pressure. The boundary conditions by the step-functions cuts  $H(\theta)$ , defining the **RAD** in the two forms of the **RAD** potential functions, will be included in the energy momentum tensor. Nevertheless, clearly the projection after  $3 + 1$  decomposition, defining the 3D hyperplane  $h_{ij}^{(i)}$ , has to be done according to the orthogonality condition defining fluids field velocity vectors  $\mathbf{u}^{(i)}$ , respectively, for the  $(i)$ -torus. These solutions create special tori surfaces from the condition on the constant pressure. Moreover, within the limits considered before, these constraints can found application also in the collision analysis, to infer the final states (es. final merger tori) from these constraints. (Other notable cases might be founded by the constraints  $\varrho_{[\times]} = \varrho_\gamma^i \varrho_\gamma^o = \text{constant}$ ,  $\varrho_{\{\times\}} = \varrho_\gamma(K^i K^o) = \text{constant}$  or  $\varrho_{\{+\}}^\pm = \varrho_\gamma(K^i \pm K^o) = \text{constant}$ .) It is possible to show that not all these profiles are related to quiescent or accreting toroids.

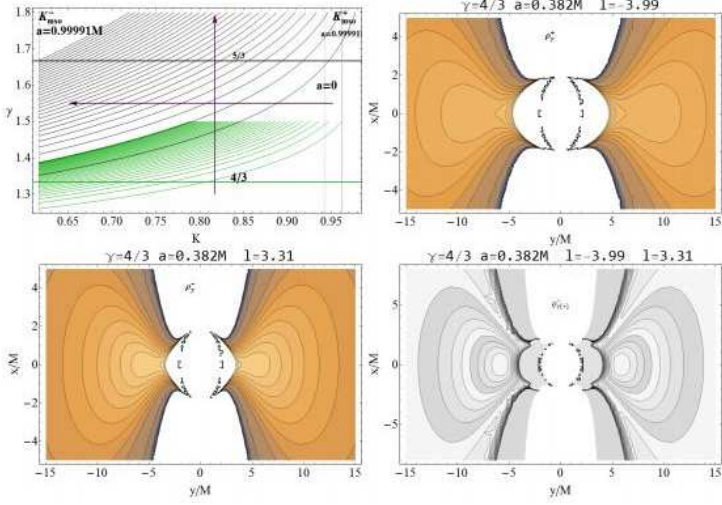


**Figure 1.** *Left panel:* Profiles of constant rationalized density function  $\rho_k$  in Eq. (3) in the plane  $\gamma - K$ ,  $\gamma > 1$  is the polytropic index,  $K \in [K_{mso}^\pm, 1]$  is the  $K$ -parameter attached to any tori at constant  $\ell$ . The values  $K_{mso}^\pm$  for the two **SMBHs** with spin  $a = 0$  and  $a = 0.99991M$  are also plotted. Corotating ([−]) and counterrotating fluids ([+]) are considered. Indices  $\gamma = 4/3$  considered also for the analysis of Pugliese and Stuchlík (2019) and  $\gamma = 5/3$  are shown. Arrows follow the increasing values of  $\rho_\gamma$ . The region in the range  $\gamma \in [4/3, 5/3]$  has been partially thickened with highlighted (green-colored)  $K$ -constant curves. Density profiles  $\rho_\gamma^\pm$  for corotating (*bottom left panel*) and counterrotating tori (*upper right panel*) orbiting around a **SMBH** with spin  $a = 0.382M$ , the fluids specific angular momentum is  $\ell = -3.99$  and  $\ell = 3.31$ , the polytropic index  $\gamma = 4/3$ .  $(x, y)$  are Cartesian coordinates. (*Bottom right panel*) profiles of constant composite density function  $\rho_{\gamma[+]}^-$  defined in Sec. (2.1).

### 3 INFLUENCE OF TOROIDAL MAGNETIC FIELD IN MULTI-ACCRETING TORI

In this section we consider **RAD** with toroidal sub-structures regulated by the presence, in the force balance equation of a toroidal magnetic field component. We refer to the analysis of Pugliese and Montani (2018), the toroidal magnetic field form used here is the well known Komissarov-solution Komissarov (2006), used in the approach Pugliese and Montani (2013, 2018), see also Adámek and Stuchlík (2013); Hamersky and Karas (2013); Karas et al. (2014); Zanotti and Pugliese (2015). In this section we use mainly dimensionless units.

#### 3.1 Ideal GR-MHD

Before considering the model of magnetized **RAD**, it is convenient to review some basic notions of ideal GR-MHD. The fluids energy-momentum tensor can be written as the

composition of the two components

$$\begin{aligned} T_{ab}^f &= (\varrho + p)U_a U_b - \epsilon p g_{ab} \\ T_{ab}^{\text{em}} &= -\epsilon \left( F_{ac} F_b^c - \frac{1}{4} F_{cd} F^{cd} g_{ab} \right) = \frac{g_{ab}}{2} (E^2 + B^2) - (E_a E_b + B_a B_b) \\ -2\epsilon \check{G}_{(a} U_{b)} - \epsilon U_a U_b (E^2 + B^2), \quad \nabla_{[a} F_{bc]} &= 0, \quad \nabla^a F_{ab} = \epsilon J_b \quad J^a = \varrho_c U^a + j^a, \end{aligned} \quad (4)$$

(quantities are measured by an observers moving with the fluid).  $\check{G}_a$  denotes the Pointing vector,  $U^a U_a = \epsilon$ , ( $\epsilon$  in this section is clearly a signature sign) and  $h_{ab} \equiv g_{ab} - \epsilon U_a U_b$ , is the projection tensor, where  $\nabla_\alpha g_{\beta\gamma} = 0$ . Considering the charge density and conduction current with the Ohm's law, there is  $j^a = \sigma^{ab} E_b$ ,  $J^a = \varrho_c U^a + \sigma E^a$ . We consider isotropic fluids for which  $\sigma^{ab} = \sigma g^{ab}$ ,  $\sigma$  is the electrical conductivity coefficient. For ideal conductive plasma there is  $\sigma \rightarrow \infty$  ( $E_a = F_{ab} U^b = 0$ ): the electromagnetic field does not have a direct effect on the conservation equation along the flow lines, or

$$\begin{aligned} U_a \nabla^a \varrho + (p + \varrho) \nabla^a U_a - U^b F_b^c (\nabla^a F_{ac}) &= 0, \\ \text{In the ideal MHD} \quad (p + \varrho) U^a \nabla_a U^c - \epsilon h^{bc} \nabla_b p - \epsilon (\nabla^a F_{ad}) F^{cd} &= 0, \\ \text{and} \quad U^a \nabla_a s &= \frac{1}{nT} U^b F_b^c \nabla^a F_{ac}. \end{aligned}$$

( $T$  is the temperature and  $n$  is the particle number density). In infinitely conducting plasma there is  $U^a \nabla_a s = 0$  the entropy per particle is conserved along the flow lines of each toroids. A particular case of interest is when  $s$  is a constant of both space and time implying  $p = p(\varrho)$ . Pugliese and Valiente Kroon (2016); Pugliese and Kroon (2012).

### 3.2 Magnetized tori

We consider, in the magnetized case, an infinitely conductive plasma where  $F_{ab} U^a = 0$ , and  $F_{ab}, U^a B_a = 0$ , and  $\partial_\phi B^a = 0$  and  $B^r = B^\theta = 0$ . The toroidal magnetic field contribution in each **RAD** component can be written by considering,

$$\begin{aligned} B^\phi &= \sqrt{\frac{2p_B}{g_{\phi\phi} + 2\ell g_{t\phi} + \ell^2 g_{tt}}} \quad \text{or alternatively} \\ B^\phi &= \sqrt{2\mathcal{M}\omega^q} (g_{t\phi} g_{t\phi} - g_{tt} g_{\phi\phi})^{(q-2)/2} V_{eff}(\ell) \end{aligned} \quad (5)$$

with  $p_B = \mathcal{M} (g_{t\phi} g_{t\phi} - g_{tt} g_{\phi\phi})^{q-1} \omega^q$  the magnetic pressure,  $\omega$  is the fluid enthalpy,  $q$  and  $\mathcal{M}$  (magnitude) are constant;  $V_{eff}$  is a function of the metric and the angular momentum  $\ell$ —Komissarov (2006); Zanotti and Pugliese (2015); Pugliese and Montani (2013); Adámek and Stuchlík (2013); Hamersky and Karas (2013); Karas et al. (2014). The Euler equation for the HD case is modified by the term:

$$\begin{aligned} \partial_\mu \tilde{W} &= \partial_\mu [\ln V_{eff} + \mathcal{G}] \quad \text{where} \quad (a \neq 0) : \mathcal{G}(r, \theta) = \mathcal{S} (\mathcal{A} V_{eff}^2)^{q-1}; \\ \text{and } \mathcal{A} &\equiv \ell^2 g_{tt} + 2\ell g_{t\phi} + g_{\phi\phi}, \quad \mathcal{S} \equiv \frac{q\mathcal{M}\omega^{q-1}}{q-1}, \end{aligned} \quad (6)$$

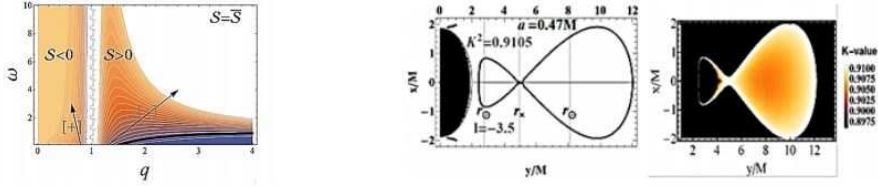


**Figure 2.** Left panel: Profiles of  $S = \text{constant}$  in the panel  $\omega$ - $q$ , where  $\omega$  is the fluid enthalpy and  $q$  is a magnetic field family parameter. Arrow directions indicate the increasing values of  $S$ .  $q = 1$  is a singular value for  $S$ . At  $q < 1$  ( $S < 0$ ) excretion tori (density profiles in the right panel) appear. From Pugliese and Montani (2018).

We here concentrate on  $q > 1$  as, the magnetic parameter  $S$  is negative for  $q < 1$ , where excretion tori are possible (Stuchlik (2005); Stuchlik et al. (2009); exc; Stuchlik and Schee (2010),  $q = 1$ , is a singular values for  $S$  —Figs (2). In this new frame, the analysis of **RAD** structure is performed by considering the new equation  $\tilde{W} \equiv \mathcal{G}(r, \theta) + \ln(V_{eff}) = K$ . The deformed potential function  $\tilde{V}_{eff}^2$ ,

$$\begin{aligned} \tilde{V}_{eff}^2 &\equiv V_{eff}^2 e^{2S(AV_{eff}^2)^{q-1}} = \\ &= \frac{(g_{t\phi}g_{t\phi} - g_{tt}g_{\phi\phi}) \exp\left(2S(g_{t\phi}g_{t\phi} - g_{tt}g_{\phi\phi})^{q-1}\right)}{\ell^2 g_{tt} + 2\ell g_{t\phi} + g_{\phi\phi}} = K^2, \end{aligned} \quad (7)$$

for  $S = 0$  (or  $\mathcal{M} = 0$ ) reduces to the effective potential  $V_{eff}^2$  for the HD case:  $V_{eff}^2$ :  $\tilde{V}_{eff}^2 = V_{eff}^2 + \frac{2S(AV_{eff}^2)^q}{A} + O(S^2)$ .

$$S_n = \frac{\mathcal{M} \ln^n(\omega)(n + \ln(\omega) + 1)}{\Gamma(n + 2)} \text{ for } n \geq 0 \text{ and } q \gtrsim 1, \quad (8)$$

where  $\Gamma(x)$  is the Euler gamma function. As for the HD case in Eq. (2), we could find the **RAD** angular momentum distribution:

$$\tilde{\ell}^\mp \equiv \frac{\Delta \left( a^3 + ar [4Q(r - M)S\Delta^\mathcal{Q} + 3r - 4] \mp \sqrt{r^3 [\Delta^2 + 4Q^2(r - 1)^2 r S^2 \Delta^{2\mathcal{Q}+1} + 2Q(r - 1)^2 r S\Delta^\mathcal{Q}]}\right)}{a^4 - a^2(r - 3)(r - 2)r - (r - 2)r [2Q(r - 1)S\Delta^\mathcal{Q} + (r - 2)^2 r]}$$

where there is  $\lim_{S \rightarrow 0} \tilde{\ell}^\mp = \lim_{q \rightarrow 1} \tilde{\ell}^\mp = \ell^\pm$ ,  $Q \equiv q - 1$

(dimensionless units)—Figs (3). However the introduction of a toroidal magnetic field  $B$ , makes the study of the momentum distribution within the disk rather complicated. Instead, in Pugliese and Montani (2018) it was adopted a function derived from the  $S$  parameter:

$$\textbf{Leading RAD function: } S_{crit} \equiv -\frac{\Delta^{-Q}}{Q} \frac{a^2(a - \ell)^2 + 2r^2(a - \ell)(a - 2\ell) - 4r(a - \ell)^2 - \ell^2 r^3 + r^4}{2r(r - 1)[r(a^2 - \ell^2) + 2(a - \ell)^2 + r^3]} \quad (10)$$

This function represents, instead of Eq. (9) the new leading function for the distribution of tori in the **RAD** having a toroidal magnetic field component (each torus is on a line



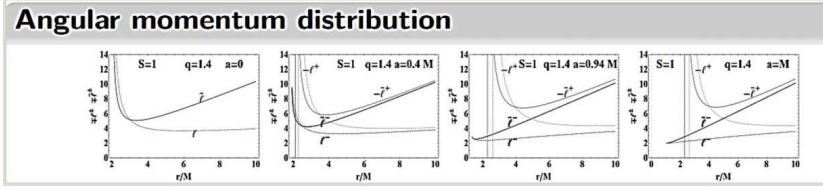


**Figure 3.** Magnetized **RAD**: angular momentum profiles  $\tilde{\ell}$  in comparison with the HD case  $\ell$ , for different values of the magnetic parameters  $S$  and  $q$  and the **BH** dimensionless spin  $a/M$ , from the Schwarzschild case  $a = 0$  to the extreme Kerr **BH**  $a = M$  for corotating (-) and counterrotating (+) fluids. From Pugliese and Montani (2018).

$S = \text{constant}$ ) and able to determine (1) the limits on the value of the magnetic parameter for the tori formation, (2) the emergence of HD instability associated with the cusped configurations  $C_{\times}$  and  $O_{\times}$ , (3) the emergence of collision between two tori of a **RAD** couple. (4) it highlights the difference between magnetized corotating and counter-rotating tori with respect to the central black hole. (This difference is also evident from the dependence in Eq. (10) from the quantities  $(a \pm \ell)$ .) As demonstrated in Pugliese and Montani (2018), such magnetized tori can be formed in the **RAD** macroconfigurations for sufficiently small  $(qS)$ , the constraints described in Sec. (A) are essentially confirmed for the magnetized case.

#### 4 CONCLUDING REMARKS

The **RAD** dynamics is strongly affected by the dimensionless spin of the central **BH** and the fluids relative rotation, especially in the magnetized case considered in Sec. (3). More generally there is evidence of a strict correlation between **SMBH** spin, fluid rotation and magnetic fields in **RADs** formation and evolution. The analysis presented here poses constraints on tori formation and emergence of **RADs** instabilities in the phases of accretion onto the central attractor and tori collision emergence (Pugliese and Stuchlík (2017, 2019)). Eventually the **RAD** frame investigation constraints specific classes of tori that could be observed around some specific **SMBHs** identified by their dimensionless spin. As a baseline result we provided a full characterization of the counterrotating tori in the multi-accreting systems. This model is designed for an extension to a dynamic GRMHD setup. From an observational viewpoint, **AGN** X-ray variability suggests a connection between X-rays and the innermost regions of the accretion disk. In Sochora et al. (2011); Karas and Sochora (2010); Schee and Stuchlík (2009); Sch. relatively indistinct excesses of the relativistically broadened emission-line components were predicted arising in a well-confined radial distance in the accretion structure originating by a series of episodic accretion events.

Another significant aspect is the possibility to relate the **RAD** oscillations of its components with **QPOs**: radially oscillating tori of the couple could be related to the high-frequency quasi-periodic oscillations (**QPOs**). Finally, for a discussion on the relation between Papaloizou-Pringle (**PP**) global incompressible modes in the tori, the Papaloizou-Pringle Instability (**PPI**), a global, hydrodynamic, non-axis-symmetric instability and the



Magneto-Rotational Instability (MRI) modes see Pugliese and Montani (2018); Bugli et al. (2018).

As an extension of this model to more general situation multi orbiting configurations are also studied considering tilted of warped disks Pugliese and Stuchlík (2017). This possibility, rather probable as a scenario in the initial phases of tori formation, could be investigated as perturbation or deformation of the axis-symmetric equatorial model considered here.

## ACKNOWLEDGEMENTS

D.P. acknowledges partial support from the Junior GACR grant of the Czech Science Foundation No:16-03564Y. Z. S. acknowledges the Albert Einstein Centre for Gravitation and Astrophysics supported by grant No. 14-37086G.

## APPENDIX A: BASIC HD-RAD CONSTRAINTS

In this section we see some main constraints of the **RAD** models by schematically summarizing the analysis of Pugliese and Stuchlík (2017, 2019).

In general, two quiescent tori (not cusped tori) can exist in all Kerr spacetimes if their specific angular momenta are properly related. Whereas there are only the following four double tori with a critical (cusped) topology: **i)**  $C_{\times}^{\pm} < C^{\pm}$  **ii)**  $C_{\times}^{+} < C^{\pm}$ , **iii)**  $C_{\times}^{-} < C^{\pm}$  and **iv)**  $C_{\times}^{-} < C_{\times}^{+}$ –

Moreover: • for  $\ell$ corotating tori or in the background of a static (Schwarzschild) attractor only the inner torus can be accreting (with a cusp). • In the  $\ell$ counterrotating couple, an cusped corotating torus has to be the inner one of the couple where the outer counterrotating torus can be in quiescent or with a cusp. If there is  $C_{\times}^{-}$  (or for a static attractor), then  $C_{\times}^{-}$  is part of  $C_{\times}^{-} < C^{-}$  or  $C_{\times}^{-} < ()^{+}$ , doubled system.

Therefore, summarizing the situation for corotating and counterrotating **RAD** components, in particular there is: • A corotating torus can be the outer of a couple with an inner counterrotating cusped surface. The outer torus of this couple may be corotating (quiescent), or counterrotating cusped or in quiescence. Both the inner corotating and the outer counterrotating torus of the couple can have a cusp. • A counterrotating torus can reach the (HD) instability as the inner configuration of an  $\ell$ corotating or  $\ell$ counterrotating couple or, viceversa, the outer torus of an  $\ell$ counterrotating couple. If the cusped torus is  $C_{\times}^{+}$ , it follows that there is no inner counterrotating torus, but there can be  $C_{\times}^{+} < C^{\pm}$  or  $()^{-} < C_{\times}^{+}$ .

## REFERENCES

- (???).  
 (???).  
 Adámek, K. and Stuchlík, Z. (2013), Magnetized tori in the field of kerr superspinars, *Classical and Quantum Gravity*, **30**(20), p. 205007.  
 Bugli, M., Guilet, J., Mller, E., Del Zanna, L., Bucciantini, N. and Montero, P. J. (2018), Papaloizou-Pringle instability suppression by the magnetorotational instability in relativistic accretion discs, *Mon. Not. Roy. Astron. Soc.*, **475**, p. 108, arXiv: 1707.01860.

- Hamersky, J. and Karas, V. (2013), Effect of the toroidal magnetic field on the runaway instability of relativistic tori, *Astron. Astrophys.*, **555**, p. A32, arXiv: 1305.6515.
- Karas, V., Kopceck, O., Kunneriath, D. and Hamersky, J. (2014), Oblique magnetic fields and the role of frame dragging near rotating black hole, *Acta Polytech.*, **54**(6), pp. 398–413, arXiv: 1408.2452.
- Karas, V. and Sochora, V. (2010), Extremal Energy Shifts of Radiation from a Ring Near a Rotating Black Hole, *The Astrophysical Journal*, **725**, pp. 1507–1515, arXiv: 1010.5785.
- Komissarov, S. S. (2006), Magnetized tori around Kerr black holes: analytic solutions with a toroidal magnetic field, *Monthly Notices of the Royal Astronomical Society*, **368**, pp. 993–1000, arXiv: astro-ph/0601678.
- Pugliese, D. and Kroon, J. A. V. (2012), On the evolution equations for ideal magnetohydrodynamics in curved spacetime, *Gen. Rel. Grav.*, **44**, pp. 2785–2810, arXiv: 1112.1525.
- Pugliese, D. and Montani, G. (2013), Squeezing of toroidal accretion disks, *EPL*, **101**(1), p. 19001, arXiv: 1301.1557.
- Pugliese, D. and Montani, G. (2015), Relativistic thick accretion disks: morphology and evolutionary parameters, *Phys. Rev.*, **D91**(8), p. 083011, arXiv: 1412.2100.
- Pugliese, D. and Montani, G. (2018), Influence of toroidal magnetic field in multiaccreting tori, *Mon. Not. Roy. Astron. Soc.*, **476**(4), pp. 4346–4361, arXiv: 1802.07505.
- Pugliese, D., Montani, G. and Bernardini, M. G. (2013), On the Polish doughnut accretion disk via the effective potential approach, *Mon. Not. Roy. Astron. Soc.*, **428**(2), pp. 952–982, arXiv: 1206.4009.
- Pugliese, D. and Stuchlík, Z. (2017), to be submitted, .
- Pugliese, D. and Stuchlík, Z. (2018a), Proto-jet configurations in RADs orbiting a Kerr SMBH: symmetries and limiting surfaces, *Class. Quant. Grav.*, **35**(10), p. 105005, arXiv: 1803.09958.
- Pugliese, D. and Stuchlík, Z. (2018b), Relating Kerr SMBHs in active galactic nuclei to RADs configurations, *Class. Quant. Grav.*, **35**(18).
- Pugliese, D. and Stuchlík, Z. (2018c), Tori sequences as remnants of multiple accreting periods of Kerr SMBHs, *JHEAp*, **17**, pp. 1–37, arXiv: 1711.04530.
- Pugliese, D. and Stuchlík, Z. (2015), Ringed accretion disks: equilibrium configurations, *Astrophys. J. Suppl.*, **221**, p. 25, arXiv: 1510.03669.
- Pugliese, D. and Stuchlík, Z. (2016), Ringed accretion disks: instabilities, *Astrophys. J. Suppl.*, **223**(2), p. 27, arXiv: 1603.00732.
- Pugliese, D. and Stuchlík, Z. (2017), Ringed accretion disks: evolution of double toroidal configurations, *Astrophys. J. Suppl.*, **229**(2), p. 40, arXiv: 1704.04063.
- Pugliese, D. and Stuchlík, Z. (2019), RADs energetics and constraints on emerging tori collisions around super-massive Kerr Black Holes, arXiv: 1903.05970.
- Pugliese, D. and Valiente Kroon, J. A. (2016), On the locally rotationally symmetric EinsteinMaxwell perfect fluid, *Gen. Rel. Grav.*, **48**(6), p. 74, arXiv: 1410.1335.
- Schee, J. and Stuchlík, Z. (2009), Profiles of emission lines generated by rings orbiting braneworld Kerr black holes, *Gen. Rel. Grav.*, **41**, pp. 1795–1818, arXiv: 0812.3017.
- Sochora, V., Karas, V., Svoboda, J. and Dovčiak, M. (2011), Black hole accretion rings revealed by future X-ray spectroscopy, *Monthly Notices of the Royal Astronomical Society*, **418**, pp. 276–283, arXiv: 1108.0545.
- Stuchlík, Z. (2005), Influence of the relict cosmological constant on accretion discs, *Mod. Phys. Lett.*, **A20**, p. 561, arXiv: 0804.2266.
- Stuchlík, Z. and Schee, J. (2010), Appearance of Keplerian discs orbiting Kerr superspinars, *Class. Quant. Grav.*, **27**, p. 215017, arXiv: 1101.3569.

- Stuchlik, Z., Slany, P. and Kovar, J. (2009), Pseudo-Newtonian and general relativistic barotropic tori in Schwarzschild-de Sitter spacetimes, *Class. Quant. Grav.*, **26**, p. 215013, arXiv: 0910.3184.
- Zanotti, O. and Pugliese, D. (2015), Von Zeipel's theorem for a magnetized circular flow around a compact object, *Gen. Rel. Grav.*, **47**(4), p. 44, arXiv: 1412.6447.

